Journal of Fluids and Structures 41 (2013) 99–108

Contents lists available at ScienceDirect

Journal of Fluids and Structures

journal homepage: www.elsevier.com/locate/jfs

Computational simulation of the flow-induced vibration of a circular cylinder subjected to wake interference

Bruno S. Carmo [a,*], Gustavo R.S. Assi [b], Julio R. Meneghini [a]

[a] Department of Mechanical Engineering, Poli, University of São Paulo, Av. Prof. Melo Morais, 2231, Cidade Universitária, São Paulo 05508-030, SP, Brazil
[b] Department of Naval Engineering, Poli, University of São Paulo, Brazil

ARTICLE INFO

Article history:
Received 30 March 2012
Received in revised form
14 January 2013
Accepted 3 February 2013
Available online 22 March 2013

Keywords:
Flow-induced vibration
Numerical simulation
Flow interference

ABSTRACT

In this work, we considered the flow around two circular cylinders of equal diameter placed in tandem with respect to the incident uniform flow. The upstream cylinder was fixed and the downstream cylinder was completely free to move in the cross-stream direction, with no spring or damper attached to it. The centre-to-centre distance between the cylinders was four diameters, and the Reynolds number was varied from 100 to 645. We performed two- and three-dimensional simulations of this flow using a Spectral/hp element method to discretise the flow equations, coupled to a simple Newmark integration routine that solves the equation of the dynamics of the cylinder. The differences of the behaviours observed in the two- and three-dimensional simulations are highlighted and the data is analysed under the light of previously published experimental results obtained for higher Reynolds numbers.

1. Introduction

The flow around circular cylinders has been extensively studied due to its practical importance in engineering and scientific relevance in fluid mechanics. When circular cylinders are grouped in close proximity, the flow field and the forces experienced by the cylinders can be entirely different from those observed when the bodies are isolated in the fluid stream. The effect of the presence of other bodies in the flow is called *flow interference*. One of the most severe types of interference, and the type on which this paper focuses, is *wake interference*, which happens when the cylinder is immersed or in close proximity to the wake of another bluff body. In such situations, the flow impinging on the cylinder is usually totally different from the free-stream. Given the number of differences observed in the forces exerted on cylinders subjected to wake interference when compared to the single cylinder case, one expects that the flow-induced vibrations (FIV) experienced by a flexible cylinder or a compliantly mounted rigid cylinder will also be different depending whether the cylinder is immersed in a vortex wake or not.

A few papers on this matter have been published, most of them were concerned with vibrations within the synchronisation range, i.e. when the vortex shedding is synchronised with the cylinder vibration. King and Johns (1976) investigated the vibration of two flexible cylinders in tandem by performing experiments in a water channel. Bokaian and Geoola (1984) carried out experiments on the flow around circular cylinders in tandem and staggered arrangements, the upstream cylinder being fixed and the downstream one being rigid and mounted on an elastic base that allowed

* Corresponding author. Tel.: +55 11 3091 9882; fax: +55 11 3091 5642.
E-mail addresses: bruno.carmo@usp.br (B.S. Carmo), g.assi@usp.br (G.R.S. Assi), jmeneg@usp.br (J.R. Meneghini).

0889-9746/$ - see front matter © 2013 Elsevier Ltd. All rights reserved.
http://dx.doi.org/10.1016/j.jfluidstructs.2013.02.010

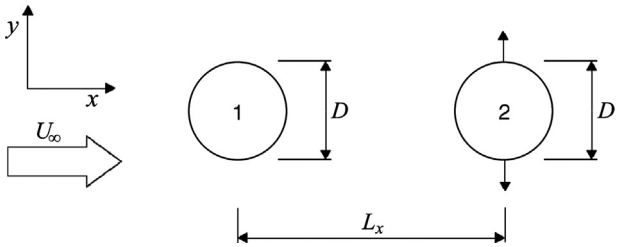

Fig. 1. Schematic drawing of arrangement studied.

cross-stream displacement. Zdravkovich (1985) investigated the behaviour of two flexible circular cylinders placed in diverse arrangements using a wind tunnel. Brika and Laneville (1999) utilised wind tunnel experiments to study the flow induced vibrations of a flexible circular cylinder, allowed to vibrate in one plane only, immersed in the wake of a rigid cylinder. Assi et al. (2006) performed experiments on the FIV of a elastically mounted rigid cylinder in the wake of a fixed identical cylinder, using a water channel. Recently, there has also been a few computational studies on FIV of two circular cylinders in tandem. Examples of this type of work are Mittal and Kumar (2001), Jester and Kallinderis (2004) and Papaioannou et al. (2008). In all these papers, the computations were two-dimensional and focused on reduced velocities within the synchronisation range. In general terms, they confirmed the main conclusions of previously published experimental data: the wake interference led to a wider synchronisation range and within this range the amplitude of response was larger than that observed in the response of an isolated cylinder with the same structural parameters.

However, some papers have also reported that cylinders subjected to wake interference also experienced vibrations with high amplitudes for higher reduced velocities, outside the synchronisation range (Bokaian and Geoola, 1984; Brika and Laneville, 1999; Hover and Triantafyllou, 2001; Zdravkovich, 1985). In most cases, the amplitude levels were even higher than those observed in the lock-in. Although the reduced velocity for which this peculiar type of response starts to be significant seems to depend on various aspects, such as the separation between the cylinders and the mass ratio, all the papers agree on the fact that an upper reduced velocity limit for which these vibrations would cease does not seem to exist.

In this paper, we investigate the limit case of this phenomenon by removing the springs and the damper attached to the downstream cylinder, i.e. making the reduced velocity equal to infinity. The arrangement is illustrated in Fig. 1: both cylinders have the same diameter, the upstream cylinder is fixed and the downstream cylinder is allowed to move in the cross-stream direction without any type of constraint. We limit our investigation to the case in which the centre-to-centre separation, L_x, is equal to $4D$, and study the influence of the Reynolds number in the range $100 \leq \mathrm{Re} \leq 645$, employing two- and three-dimensional numerical simulations.

2. Numerical method

The computational results were obtained by coupling the solution of the flow with the solution of the structural response. The flow is governed by the incompressible Navier–Stokes equations, which can be written in non-dimensional form as

$$\frac{\partial \mathbf{u}}{\partial t} = -(\mathbf{u}.\nabla)\mathbf{u} - \nabla p + \frac{1}{\mathrm{Re}}\nabla^2\mathbf{u}, \tag{1}$$

$$\nabla.\mathbf{u} = 0. \tag{2}$$

The cylinder diameter D is the reference length and the free-stream speed U_∞ is the reference speed used in the non-dimensionalisation. $\mathbf{u} \equiv (u,v,w)$ is the velocity field, t is the time, p is the static pressure, $\mathrm{Re} = \rho U_\infty D/\mu$ is the Reynolds number and μ is the dynamic viscosity of the fluid. The pressure was assumed to be scaled by the constant density ρ. The numerical solution of these equations was calculated using a Spectral/hp discretisation as described in Karniadakis and Sherwin (2005).

On the structural side, we assumed that the moving cylinder was rigid and free to move in only one direction. The response of the cylinder to an external force is governed by Newton's second law, written in non-dimensional form as

$$\frac{\pi m^*}{4}\ddot{y}_c^* = F_y^*(\ddot{y}_c^*, \dot{y}_c^*, y_c^*, t^*). \tag{3}$$

In this equation, $m^* = 4M/(\rho\pi D^2 L)$ is the mass ratio, $F_y^* = C_L/2 = F_y/(\rho U_\infty^2 DL)$ is the non-dimensional force imposed by the fluid in the direction of motion. L is the (axial) length of the cylinder and C_L is the lift coefficient. The variables $\ddot{y}_c^*$, $\dot{y}_c^*$, y_c^* are the non-dimensional acceleration, velocity and displacement of the body, respectively, and t^* is the non-dimensional time.

These variables are non-dimensionalised according to the expressions

$$\ddot{y}_c^* = \frac{\ddot{y}_c D}{U_\infty^2}, \quad \dot{y}_c^* = \frac{\dot{y}_c}{U_\infty}, \quad y_c^* = \frac{y_c}{D}, \quad t^* = \frac{tU_\infty}{D}.$$

The structural equation was integrated using Newmark's (1959) scheme.

The fluid–structure interaction problem this paper is concerned with comprises the flow around two bodies, with one of them being allowed to move independently of the other. The computational code used to simulate the flow had to provide support for that, thus an Arbitrary Lagrangian–Eulerian (ALE) formulation was employed. The ALE formulation consists basically in incorporating arbitrary displacements of the mesh into the equations being solved, so the movement of the bodies and the mesh deformations necessary to maintain an adequate spatial discretisation can be taken into account. This can be achieved by doing a simple modification in the advection term of the incompressible Navier–Stokes equations (1) and (2),

$$\frac{\partial \mathbf{u}}{\partial t} = -(\mathbf{u}-\mathbf{m}) \cdot \nabla \mathbf{u} - \nabla p + \frac{1}{\mathrm{Re}} \nabla^2 \mathbf{u}, \tag{4}$$

$$\nabla \cdot \mathbf{u} = 0, \tag{5}$$

where $\mathbf{m}$ is the velocity of the mesh. The velocity of the mesh on the cylinder walls was given by the velocity of the bodies and was zero on the other boundaries of the domain. The velocity of the mesh in the interior of the domain was calculated in an automated way following the scheme presented by Batina (1990). Eqs. (4) and (5) are the Arbitrary Lagrangian–Eulerian form of the Navier–Stokes equations.

Eqs. (3)–(5) have to be solved in a coupled manner. The fluid load F_y^* in Eq. (3) is calculated from the solution of the flow (4) and (5), and the motion of the boundaries, which are necessary for the solution of Eqs. (4) and (5), is determined by the solution of the structure Eq. (3). The equations were integrated in time employing a modified version of the algorithm described in Carmo et al. (2011). The modification consisted in the effectuation of sub-iterations so as to make the algorithm tightly coupled. In other words, sub-iterations were performed in order to assure that the body displacement and fluid force were consistent within the time-step. This measure made the code to run slower but was necessary to the integration to converge, since the increase in Reynolds number appears to make the simulation more sensitive to the low mass-ratio instability that takes place in flow–structure interaction calculations (Causin et al., 2005; Förster et al., 2007).

3. Numerical simulations

Two- and three-dimensional simulations were performed for the tandem arrangement with centre-to-centre separation $L_x/D = 4$. This separation was chosen because we were interested in investigating flows in which there is a complete wake in the region between the cylinders (the *WG* regime described in Carmo et al., 2010a) with high vibration amplitude, and previous tests with fixed cylinders showed that this configuration exhibited the desired shedding regime with high lift coefficient amplitude. The mesh employed for all the simulations is shown in Fig. 2. It extended 36*D* upstream of the upstream cylinder, the lateral boundaries were located 50*D* from the upstream cylinder centre and the outflow boundary located 45*D* from the downstream cylinder. No-slip boundary conditions were enforced on the cylinder walls, essential boundary conditions $(u,v) = (1,0)$ were enforced on the lateral and upstream boundaries, and outflow

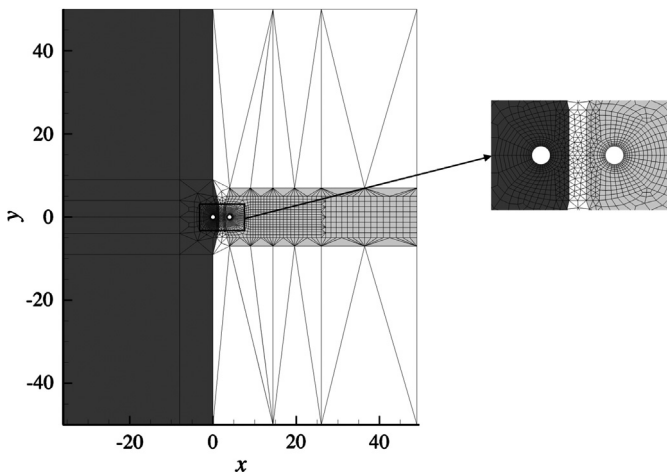

Fig. 2. Example of a mesh used with the ALE formulation, showing also the detail of the discretisation close to the cylinders. The dark grey region remains fixed, the elements in the light grey region move rigidly with the downstream cylinder and the elements in the white region deform to comply with the movement of the cylinder.

boundary conditions $(\partial u/\partial \mathbf{n}, \partial v/\partial \mathbf{n}) = (0,0)$ were employed on the downstream boundary. The high-order pressure boundary conditions were enforced on the cylinder walls, upstream and lateral boundaries, while the pressure was fixed to $p=0$ on the downstream boundary. For the three-dimensional simulations, the spanwise length of the domain was $15D$ discretised with 64 Fourier modes, and periodic boundary conditions were employed on the planes that crossed the ends of the cylinder. The mass ratio was $m^* = 2.0$ for all calculations.

The Reynolds numbers tested varied between 90 and 645 for the two-dimensional simulations and between 300 and 600 for the three-dimensional simulations. The polynomial order of the basis functions varied from 3 (lowest Reynolds numbers) to 9 (highest Reynolds numbers) for the two-dimensional simulations and from 4 to 6 for the three-dimensional simulations. We also used different time-steps according to the Reynolds number, varying from $\Delta t = 7.4 \times 10^{-3}$ for $\mathrm{Re} = 90$ to $\Delta t = 7.6 \times 10^{-4}$ for $\mathrm{Re} = 645$.

4. Results

4.1. Two-dimensional simulations

Fig. 3 shows the amplitude of response (rms of the amplitude signal multiplied by $\sqrt{2}$) obtained with the numerical simulations. It is possible to identify three different regimes in the curve relative to the two-dimensional simulations.

The first regime shows a monotonically decreasing amplitude with increasing Reynolds number, comprising the range $90 \leq \mathrm{Re} \leq 165$. It is interesting to note that for this Reynolds number range, the flow around a tandem arrangement with fixed cylinders with $L_x/D = 4$ is basically two-dimensional – the critical Reynolds number regarding three-dimensional instabilities for this arrangement is $\mathrm{Re} = 163.5$ (Carmo et al., 2010b). Fig. 5(a) shows the time history of the downstream cylinder lift coefficient and displacement. It can be seen that both the force and the displacement are harmonic, with no amplitude modulation for neither quantity. The displacement signal is always in anti-phase with respect to the force signal. Comparing the power spectral density (PSD) of the force on the upstream cylinder (Fig. 4(a)) to the PSD of the downstream cylinder displacement (Fig. 4(b)), it can be seen that the power of these two signals is concentrated at the same frequency, i.e. the displacement of the downstream cylinder is synchronised with the shedding of the upstream cylinder. The vorticity contours depicted in Fig. 5(b) show that the vortices shed from the downstream cylinder form two separated rows of vortices that interact only far downstream, more than $8D$ away from the downstream cylinder (therefore, not visible in the figure).

The second regime starts at $\mathrm{Re} \approx 180$ and is observed for Reynolds numbers up to 360. The amplitude of vibration for this regime exhibits significant scatter, as can be seen in Fig. 3. The displacement time history for this regime displays a slow modulation, as shown in Fig. 6(a). Nonetheless, the downstream cylinder displacement and upstream cylinder lift coefficient signals remain synchronised, as shown in Fig. 4. It can be seen in the vorticity contours in Fig. 6(b) that the vortices in the wake of the downstream cylinder interact in a region approximately $6D$ away from the downstream body, i.e. much closer to the bodies than for the first regime (at lower Reynolds numbers).

There is a gradual transition between the second and third regimes, happening for $360 \leq \mathrm{Re} \leq 405$. The third regime then extends up to the highest Reynolds number tested. For this regime, Fig. 3 shows that the amplitude grows monotonically with the Reynolds number. The PSD contours of the displacement of the downstream cylinder (Fig. 4(b)) shows that for this regime there is a strong component at low frequencies and this component does not have

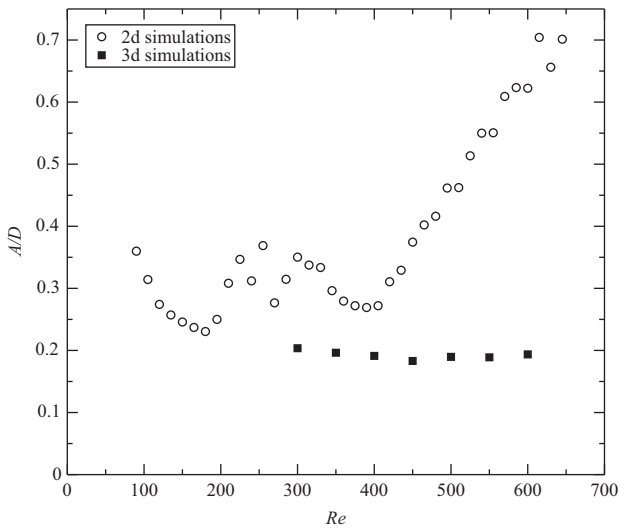

Fig. 3. Response amplitude obtained from two- and three-dimensional simulations at different Reynolds numbers.

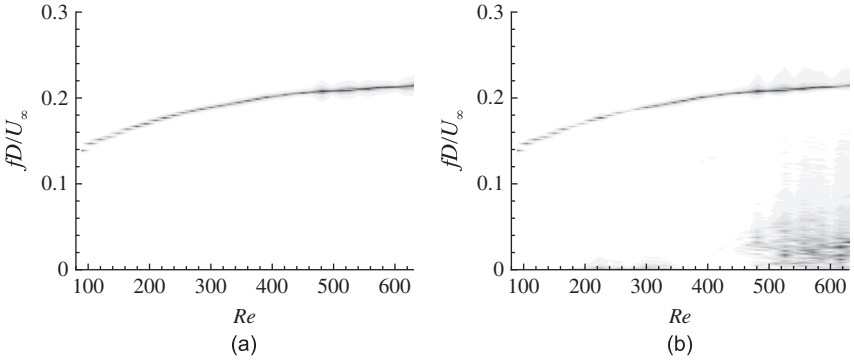

Fig. 4. Contours of normalised power spectral density of the upstream cylinder lift coefficient and downstream cylinder displacement, as functions of the Reynolds number; two-dimensional simulations. (a) Upstream cylinder C_L. (b) Downstream cylinder y_c.

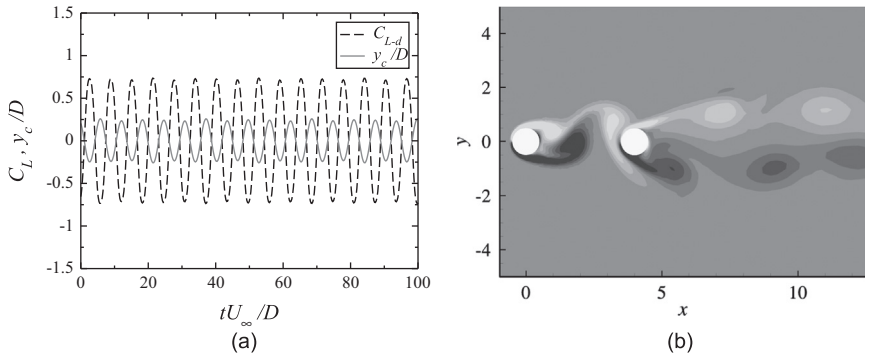

Fig. 5. Downstream cylinder lift coefficient and displacement time series (a) and instantaneous vorticity contours (b); Re = 150, two-dimensional simulations.

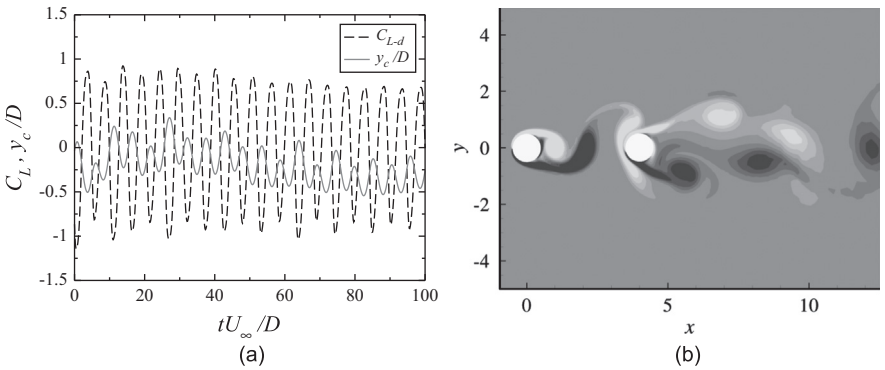

Fig. 6. Downstream cylinder lift coefficient and displacement time series (a) and instantaneous vorticity contours (b); Re = 300, two-dimensional simulations.

a corresponding match in the PSD contours of the lift of the upstream cylinder (Fig. 4(a)). The time history of the lift coefficient and displacement of the downstream cylinder, shown in Fig. 7(a), exhibit a very erratic behaviour. We see in Fig. 7(b) that the vortices in the near wake of the downstream cylinder, more precisely between the base region of the cylinder up to 4*D* downstream, but without a regular pattern.

In order to better understand why in the third regime the downstream cylinder exhibits a significant part of its oscillation power at low frequencies, let us analyse the response of a mass-spring-damper system to a oscillatory force. In this case, the motion of the body is governed by the equation,

$$\ddot{y}_c + 2\zeta\omega_0\dot{y}_c + \omega_0^2 y_c = \frac{F_0 \sin(\omega t)}{M},$$

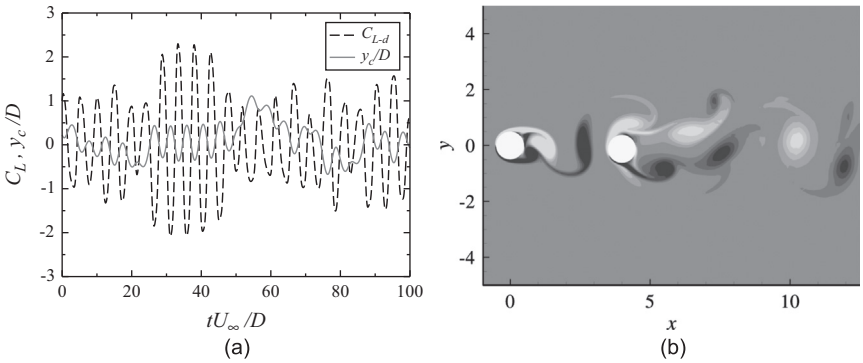

Fig. 7. Downstream cylinder lift coefficient and displacement time series (a) and instantaneous vorticity contours (b); Re = 540, two-dimensional simulations.

where $\omega_0 = \sqrt{k/m}$ is the natural frequency of the structure in vacuum and F_0 and ω are the force amplitude and frequency, respectively. After the initial transient is finished, the structure will respond according to

$$y_c(t) = \frac{F_0}{M\omega\sqrt{\left(\frac{C}{M}\right)^2 + \frac{(\omega_0^2-\omega^2)^2}{\omega^2}}}\ \sin(\omega t+\phi),$$

with

$$\phi = \arctan\left(\frac{2\omega\omega_0\zeta}{\omega^2-\omega_0^2}\right).$$

Considering that our system does not have a spring (k=0), so $\omega_0 = 0$, nor a damper (C=0), the response amplitude obeys the equation

$$A = \frac{F_0}{M\omega^2}, \tag{6}$$

from this we conclude that the amplitude of vibration of the structure will be larger if the frequency of the force is low. A generic force can be decomposed into its Fourier components and the system will respond with larger amplitudes to that components with low frequency.

The spectra of the downstream cylinder lift coefficient and displacement for diverse Reynolds numbers are plotted in Fig. 8. It can be seen that at the laminar regime (Fig. 8(a)), the force signal is harmonic, showing a very clean spectrum, so the response of the structure is also harmonic, displaying peaks only at the shedding frequency and its third harmonic. If the Reynolds number is increased (Figs. 8(b)–(d)), the signal of the force on the downstream cylinder starts to show a multitude of components due to the now turbulent wake that impinges on the downstream cylinder, although a very clear peak is still observed at the shedding frequency. Consequently, the structure then responds with larger amplitudes at the low frequency range of the spectrum, and this is basically the reason why a significant part of the power is concentrated at the low frequencies for higher Reynolds numbers, as shown in Fig. 4(b).

The origin of the third harmonic can be understood by considering that a periodic function $f(t)$ of zero mean value and period T can be represented by a Fourier series of the form:

$$f(t) = \sum_{n=1}^{\infty} a_n\ \sin(n\omega t) + b_n\ \cos(n\omega t).$$

The terms a_n and b_n of this series are given by

$$a_n = \frac{2}{T}\int_0^T f(t)\ \sin(n\omega t)\,\mathrm{d}t \quad b_n = \frac{2}{T}\int_0^T f(t)\ \cos(n\omega t)\,\mathrm{d}t.$$

By choosing the initial time appropriately, the function can be made odd, that is $f(-t) = -f(t)$. For odd functions, b_n=0 for every n. Furthermore, $f(t) = -f(t+T/2)$, hence a_n=0 for even values of n. Therefore, the function $f(t)$ can be represented by

$$f(t) = a_1\ \sin(\omega t) + a_3\ \sin(3\omega t) + a_5\ \sin(5\omega t) + \cdots, \tag{7}$$

and the number of harmonics necessary to represent $f(t)$ depends on how different from a sinusoidal function $f(t)$ is. In the cases investigated in this paper (two- and three-dimensional), both the displacement and the force signals are periodic with zero mean, but they are not perfectly sinusoidal. So Eq. (7) indicates that the odd numbered harmonics should be strong in the spectra, and this is what we observe.

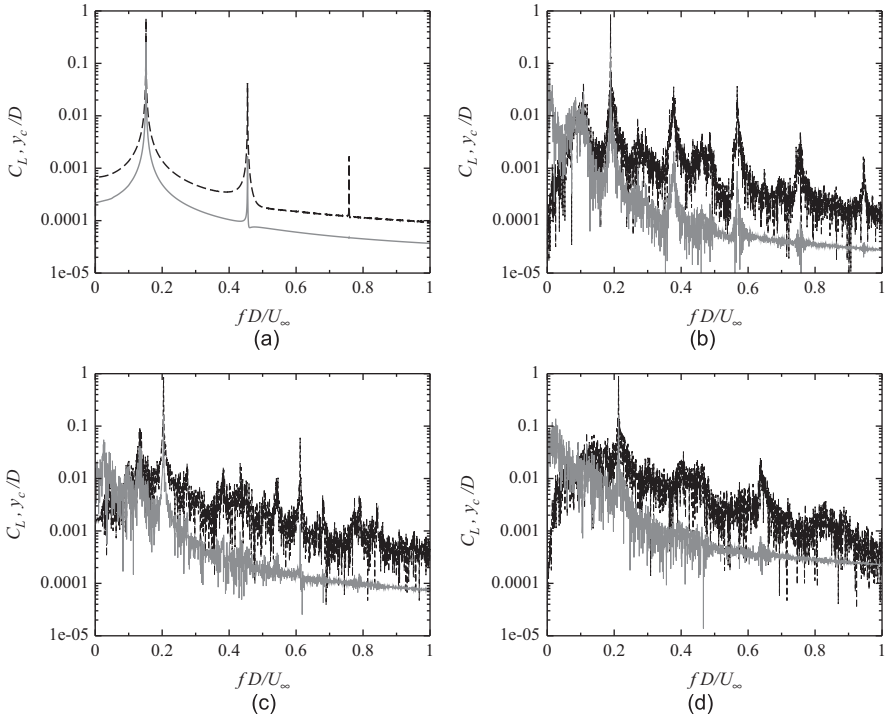

Fig. 8. Spectra for the downstream cylinder lift coefficient (dashed black lines) and displacement (solid grey lines) for various Reynolds numbers, obtained from two-dimensional simulations. (a) Re=120, (b) Re=300, (c) Re=420 and (d) Re=600.

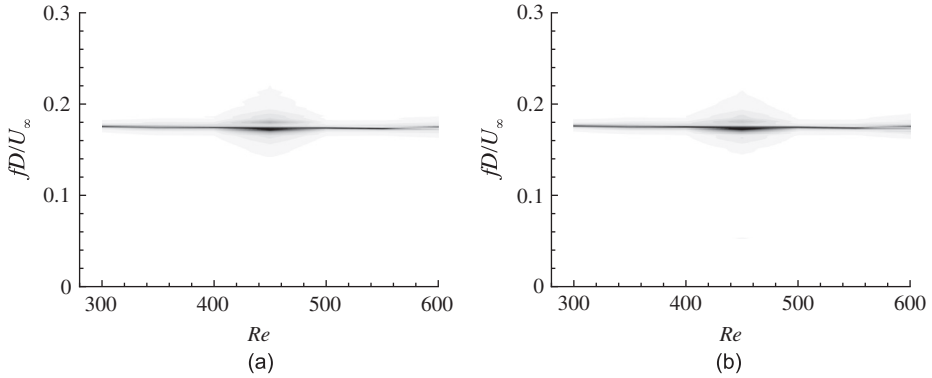

Fig. 9. Contours of normalised power spectral density of the upstream cylinder lift coefficient and downstream cylinder displacement, as functions of the Reynolds number; three-dimensional simulations. (a) Upstream cylinder C_L. (b) Downstream cylinder y_c.

4.2. Three-dimensional simulations

Fig. 3 shows that the amplitude of vibration varies very little for the three-dimensional simulations, within the Reynolds number range tested. The same can be said regarding the frequency of vibration: Fig. 9 shows that the frequency of vibration of the downstream cylinder and the frequency of shedding of the upstream cylinder are basically constant and have the same value for the entire Reynolds number range.

The time history of the downstream cylinder lift and displacement and the vorticity contours observed in the results of the three-dimensional results display very similar behaviour. Fig. 10 illustrates this behaviour by displaying these plots for Re = 400. The time histories in Fig. 10(a) show that both the lift coefficient and displacement signals exhibit a little modulation in their amplitudes. This amplitude is less strong than those observed for the second and third regimes of the two-dimensional result, and for every cycle the cylinder crosses the line $y=0$, which is not the case for the two-dimensional simulations (see Figs. 6(a) and 7(a)). Fig. 10(b) shows clearly that the spanwise vortices diffuse much more quickly if three-dimensional flow is considered. It can be seen in Fig. 11 that the wake is strongly three-dimensional, with considerable streamwise vorticity present both in the region between the cylinders and in the wake of the downstream

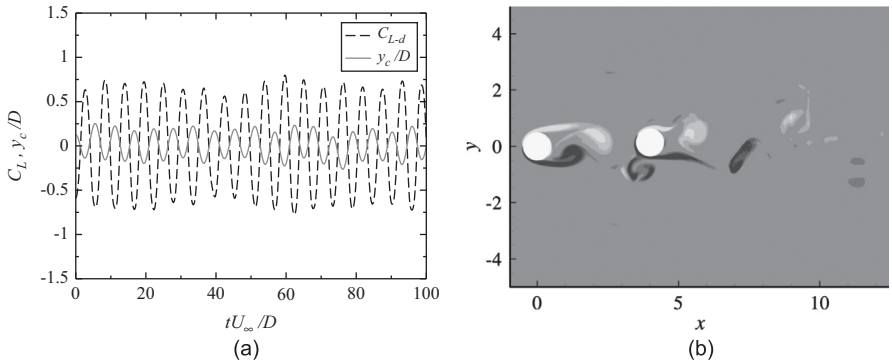

Fig. 10. Downstream cylinder lift coefficient and displacement time series (a) and instantaneous vorticity contours at $z/D = 7.5$ (b); Re = 400, three-dimensional simulations.

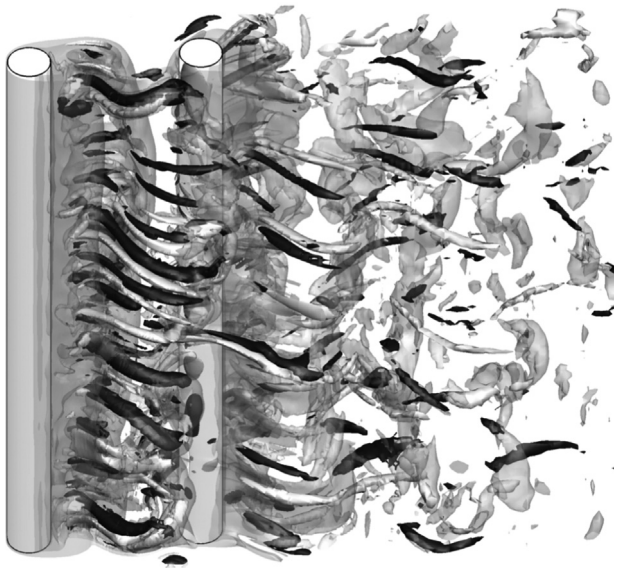

Fig. 11. Instantaneous iso-surfaces of spanwise vorticity (translucent surfaces) and streamwise vorticity (solid surfaces) for Re = 400, three-dimensional simulation. Solid light grey and dark grey surfaces represent iso-surfaces of negative and positive ω_x, respectively.

cylinder. This weakening of the spanwise vortices seems to be the main responsible for the fact that the amplitudes observed in the three-dimensional results are smaller than those observed in the two-dimensional results, for the same Reynolds numbers. Besides that, it is interesting to highlight that the amplitude level obtained from the three-dimensional calculations stays at roughly the same level, while experimental results for subcritical Reynolds numbers show growing values with increasing Reynolds numbers (Assi, 2009). We suggest that this disparity of behaviours is due to fundamental differences in the flow regimes. Once the wake is three-dimensional, an increase of Reynolds number causes two opposite effects. The first is an increase of the vortex strength, due to an increase of the vorticity magnitude of the boundary layers and consequently of the free shear layers. The second is the intensification of the three-dimensional character of the flow and turbulence in the wake, which contributes for a faster diffusion of the spanwise vorticity. The work by Noca et al. (1998) indicates that the second effect prevails over the first for $\mathrm{Re} \lesssim 1500$ and the first effect prevails over the second for $\mathrm{Re} \gtrsim 1500$. Since the forces on the downstream cylinder are directly linked to the strength of the vortices reaching the body, it is expected that the amplitude will only grow if the strength of the vortices shed by the upstream cylinder increases, i.e. if the Reynolds number is increased beyond the threshold $\mathrm{Re} \approx 1500$.

As the structural parameters did not change from the two-dimensional simulations, we still expect that the amplitude of response will be given by Eq. (6). In order to analyse the three-dimensional results using this equation, the spectra of the downstream cylinder lift coefficient and displacement were plotted for a number of different Reynolds numbers in Fig. 12. The graphs show that for all the cases the force is composed by diverse components, but the peaks at the shedding frequency and its third harmonic are clearly dominant and more pronounced than in the two-dimensional results (Fig. 8). It is important to note that the turbulent diffusion is higher in the three-dimensional simulations, because in these calculations all the components of the Reynolds stresses, combining the three velocity components, are taken into account,

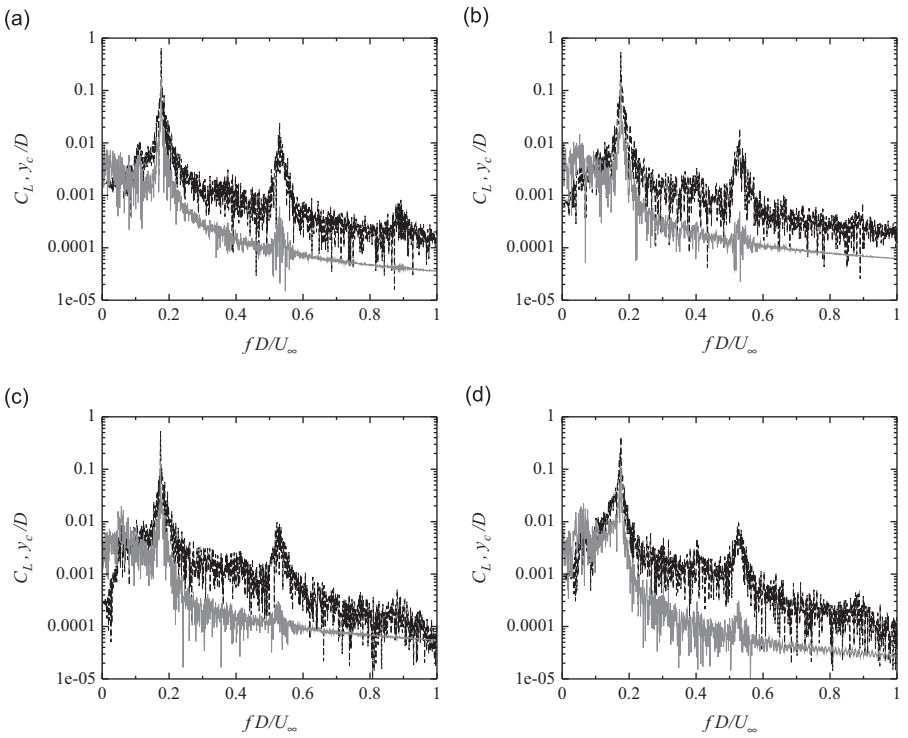

Fig. 12. Spectra for the downstream cylinder lift coefficient (dashed black lines) and displacement (solid grey lines) for various Reynolds numbers, obtained from three-dimensional simulations. (a) Re = 300, (b) Re = 400, (c) Re = 500 and (d) Re = 600.

as well as vortex stretching and vortex tilting. As a result, the flow reaching the downstream cylinder has less energy at the lower frequencies. As a consequence of these characteristics of the force signal, the cylinder response also shows marked peaks at the shedding frequency and its third harmonic. However, it is also clear that a significant part of the displacement energy is concentrated at the lower frequencies, and the importance of this part of the spectrum increases with the Reynolds number. This trend is consistent with what is observed in the experiments performed at moderate Reynolds numbers (Assi, 2009), in which most of the energy is concentrated at low frequencies of vibration.

5. Conclusion

In this paper, we have investigated the flow-induced vibration of a circular cylinder subjected to wake interference, at infinite reduced velocities. The results confirm that the presence of the wake upstream of the cylinder lead to higher amplitudes of vibration when compared to vortex-induced vibration (VIV). Furthermore, it was shown that, differently than what is observed for VIV with mass ratios above the critical value found by Govardhan and Williamson (2002), there is not a delimited range of reduced velocities for which the vibration occurs with significant amplitude. We have highlighted the differences between the results obtained with two- and three-dimensional simulations and suggested explanations for the behaviours observed. In the near future, we will try to stretch the Reynolds number range to reach values up to 2000, so as to have a more complete picture of the response of the cylinder from the onset of the transition in the wake ($Re \approx 150$) until the end of the crisis in the lift coefficient ($Re \approx 2000$).

Acknowledgment

Bruno S. Carmo would like to acknowledge the support from FAPESP through grant 2011/00131-2.

References

Assi, G.R.S., 2009. Mechanisms for Flow-Induced Vibration of Interfering Bluff Bodies. Ph.D. Thesis, Imperial College London.
Assi, G.R.S., Meneghini, J.R., Aranha, J.A.P., Bearman, P.W., Casaprima, E., 2006. Experimental investigation of flow-induced vibration interference between two circular cylinders. Journal of Fluids and Structures 22, 819–827.
Batina, J.T., 1990. Unsteady euler airfoil solutions using unstructured dynamic meshes. AIAA Journal 28, 1381–1388.
Bokaian, A., Geoola, F., 1984. Wake-induced galloping of two interfering circular cylinders. Journal of Fluid Mechanics 146, 383–415.

Brika, D., Laneville, A., 1999. The flow interaction between a stationary cylinder and a downstream flexible cylinder. Journal of Fluids and Structures 13, 579–606.
Carmo, B.S., Meneghini, J.R., Sherwin, S.J., 2010a. Possible states in the flow around two circular cylinders in tandem with separations in the vicinity of the drag inversion spacing. Physics of Fluids 22, 054101.
Carmo, B.S., Meneghini, J.R., Sherwin, S.J., 2010b. Secondary instabilities in the flow around two circular cylinders in tandem. Journal of Fluid Mechanics 644, 395–431.
Carmo, B.S., Sherwin, S.J., Bearman, P.W., Willden, R.H.J., 2011. Flow-induced vibration of a circular cylinder subjected to wake interference at low Reynolds number. Journal of Fluids and Structures 27, 503–522.
Causin, P., Gerbeau, J., Nobile, F., 2005. Added-mass effect in the design of partitioned algorithms for fluid–structure problems. Computer Methods in Applied Mechanics and Engineering 194, 4506–4527.
Förster, C., Wall, W.A., Ramm, E., 2007. Artificial added mass instabilities in sequential staggered coupling of nonlinear structures and incompressible viscous flows. Computer Methods in Applied Mechanics and Engineering 196, 1278–1293.
Govardhan, R., Williamson, C.H.K., 2002. Resonance forever: existence of a critical mass and an infinite regime of resonance in vortex-induced vibration. Journal of Fluid Mechanics 473, 147–166.
Hover, F.S., Triantafyllou, M.S., 2001. Galloping response of a cylinder with upstream wake interference. Journal of Fluids and Structures 15, 503–512.
Jester, W., Kallinderis, Y., 2004. Numerical study of incompressible flow about transversely oscillating cylinder pairs. Journal of Offshore Mechanics and Arctic Engineering—Transactions of the ASME 126, 310–317.
Karniadakis, G.E., Sherwin, S.J., 2005. Spectral/hp Element Methods for Computational Fluid Dynamics, 2nd edition Oxford University Press, Oxford, UK.
King, R., Johns, D.J., 1976. Wake interaction experiments with two flexible circular cylinders in flowing water. Journal of Sound and Vibration 45, 259–283.
Mittal, S., Kumar, V., 2001. Flow-induced oscillations of two cylinders in tandem and staggered arrangements. Journal of Fluids and Structures 15, 717–736.
Newmark, N.M., 1959. A method of computation for structural dynamics. Journal of the Engineering Mechanics Division of ASCE 85, 67–94.
Noca, F., Park, H.G., Gharib, M., 1998. Vortex formation length of a circular cylinder ($300 < Re < 4000$) using DPIV. In: Bearman, P.W., Williamson, C.H.K. (Eds.), Proceedings of Bluff Body Wakes and Vortex-Induced Vibration, ASME Fluids Engineering Division, Washington, DC, pp. 46.
Papaioannou, G.V., Yue, D.K.P., Triantafyllou, M.S., Karniadakis, G.E., 2008. On the effect of spacing on the vortex-induced vibrations of two tandem cylinders. Journal of Fluids and Structures 24, 833–854.
Zdravkovich, M.M., 1985. Flow-induced oscillations of two interfering circular cylinders. Journal of Sound and Vibration 101, 511–521.